

Effects of new non-linear couplings in relativistic effective field theory

M. Del Estal, M. Centelles, X. Viñas and S.K. Patra

*Departament d'Estructura i Constituents de la Matèria, Facultat de Física,
Universitat de Barcelona, Diagonal 647, E-08028 Barcelona, Spain*

Abstract

We extend the relativistic mean field theory model of Sugahara and Toki (TM1) by adding new couplings suggested by modern effective field theories. An improved set of parameters (TM1*) is developed with the goal to test the ability of the models based on effective field theory to describe the properties of finite nuclei and, at the same time, to be consistent with the trends of Dirac–Brueckner–Hartree–Fock calculations at densities away from the saturation region. We compare our calculations with other relativistic nuclear force parameters for various nuclear phenomena.

PACS: 21.60.-n, 21.10.Dr, 21.65.+f, 21.30.Fe

Keywords: Relativistic mean field approach, Effective field theory, Non-linear self-interactions, Dirac–Brueckner–Hartree–Fock, Nuclear structure

1 Introduction

In the recent decades relativistic quantum field theory has been very successful for the description of the nuclear many-body problem [1,2,3,4,5]. The relativistic models take care *ab initio* of many natural phenomena which are practically absent or have to be included in an *ad hoc* manner in the non-relativistic formalism. Specifically, the relativistic mean field (RMF) treatment of quantum hadrodynamics (QHD) [6,7] has become a popular way to deal with the nuclear physics problems. The original linear $\sigma - \omega$ model of Walecka [8] was complemented with cubic and quartic non-linearities of the σ meson [9] (non-linear $\sigma - \omega$ model) to improve the incompressibility and the finite nuclei results. Since these models were proposed to be renormalizable, the scalar self-interactions were limited to a quartic polynomial and scalar-vector and vector-vector interactions were not allowed. Very recently, however, inspired by effective field theory (EFT), Furnstahl, Serot and Tang [10,11] abandoned the idea of renormalizability and extended the RMF theory by allowing other non-linear scalar-vector and vector-vector self-interactions in addition to tensor couplings [7,10,11,12].

The effective field theory contains all the non-renormalizable couplings consistent with the underlying symmetries of QCD. Since one has to deal with an effective Lagrangian with an infinite number of terms it is imperative to develop a suitable expansion scheme. In the nuclear many-body problem the scalar (Φ) and vector (W) meson fields are normally small as compared with the nucleon mass (M) and they vary slowly in finite nuclei. This means that the ratios Φ/M , W/M , $|\nabla\Phi|/M^2$ and $|\nabla W|/M^2$ are the useful expansion parameters [7,10,11,12]. The concept of naturalness [7,11], i.e., that all the coupling constants written in an appropriate dimensionless form should be of the order of unity, is used to avoid ambiguities in the expansion. Then one can estimate the contributions coming from different terms by counting powers in the expansion parameters and truncating the Lagrangian at a given level of accuracy. For the truncation to be consistent, the coupling constants should exhibit naturalness and none should be arbitrarily dropped out to the given order without additional symmetry arguments.

If the EFT Lagrangian is truncated at fourth order one recovers the standard non-linear $\sigma - \omega$ model plus some additional couplings [7,11], with thirteen free parameters. In Ref. [11] these parameters have been fitted (sets G1 and G2) to reproduce twenty-nine finite nuclei observables (binding energies, charge form factors and spin-orbit splittings of magic nuclei). The fits display naturalness and the results are not dominated by the last terms retained.

This evidence confirms the utility of the EFT concepts and of the naturalness assumption, and shows that truncating the effective Lagrangian at the first lower orders is justified. The EFT approach has also been helpful to elucidate the empirical success of the usual non-linear $\sigma - \omega$ models that have less free parameters. It has been shown that the mean field phenomenology of bulk and single-particle nuclear observables does not constrain all of the parameters of the EFT model unambiguously. That is, the constants in the EFT model are underdetermined by the observables included in the fits and several parameter sets with low χ^2 can be found [7,11,13,14,15]. An analysis of the particular impact of each one of the new couplings arising in EFT on the determination of the saturation properties of nuclear matter and on the nuclear surface properties has been carried out in Ref. [16]. Recent applications of the EFT-based models include studies of pion-nucleus scattering [14], the nuclear spin-orbit force [17] and asymmetric nuclear matter at finite temperature [18].

On a more microscopic level, it is well known that non-relativistic Brueckner–Goldstone calculations based on realistic NN potentials are not able to give the right saturation density and binding energy of infinite nuclear matter at the same time (Coester line) [19]. To obtain relatively correct values an additional repulsive part has to be added. This can be achieved by working in the relativistic framework: the Dirac–Brueckner–Hartree–Fock (DBHF) theory [1,2,3,4,5,20] introduces an extra density dependence that allows to fit the NN phase shifts and to approach the empirical equilibrium point of nuclear matter. The large scalar and time-like vector self-energies of the DBHF calculations show two interesting features: a rather small effect of the two-body correlations and a weak momentum dependence, at least for not very high densities. This suggests fitting the nuclear matter DBHF self-energies by a much simpler RMF approach. This strategy was carried out in the past using the $\sigma - \omega$ model with scalar self-interactions [21,22], and also including a quartic vector self-interaction [23] (as proposed by Bodmer [24]). The outcoming parameter sets did not properly reproduce the properties of finite nuclei. The saturation properties were close to those of DBHF and it is known that they are not accurate enough, in spite of the significant improvement over the non-relativistic BHF results.

Refs. [21,22,23] showed that the success of the usual RMF model with only scalar self-interactions for describing the saturation point and the data for finite nuclei is not followed by a proper description of the trends of the DBHF scalar and vector self-energies. This is caused mainly by a too restrictive treatment of the ω -meson term: while in the standard RMF model the vector potential increases linearly with density and gets stronger, in DBHF

it bends down with density (see Figure 1 later). Moreover, the scalar potential overestimates the DBHF result at high density in order to compensate for the strong repulsion in the vector channel. This is the reason for providing the wrong sign in the coupling constant of the Φ^4 term in most of the successful RMF parameter sets. Furthermore, the equation of state becomes much steeper and soon separates from the DBHF tendency when the density grows (see Figure 2). Adding a quartic vector self-interaction remarkably improves the behaviour of the vector and scalar potentials, softens the equation of state and brings about a positive sign for the Φ^4 coupling [23,24,25]. In particular, Sugahara and Toki [25] took into account the non-linear term (W^4) in the ω vector field and fitted the free parameters to the data for several nuclei. Even with inclusion of the W^4 term they could not get with a single parametrization, and at the same time, a positive coupling constant of the Φ^4 term and a quality for nuclei along the periodic table similar to that of NL1 [26]. Thus they constructed two parameter sets, TM1 and TM2, both with a positive Φ^4 coupling constant. The TM2 set was designed for charge numbers $Z \leq 20$ and the TM1 set for larger Z . TM1 was also applied to calculate the equation of state and the structure of neutron stars and supernovae [25,27]. Apart from giving good results for finite nuclei of $Z \geq 20$, TM1 agreed with the trends of the nuclear matter DBHF calculations much better than the conventional non-linear $\sigma - \omega$ sets (such as NL1 [26] or NL3 [28]) owing to the vector self-interaction.

From the point of view of effective field theory [7,11] the models of Refs. [23,24,25,27] that include up to a quartic vector self-interaction have the drawback that the coefficients of some couplings, which should otherwise be present in the effective Lagrangian truncated at fourth order, have been put equal to zero without theoretical justification. This fact motivates us to include the remaining terms and to study their effect on nuclear matter and finite nuclei. We will show that it is possible to extend the TM1 set to describe the finite nuclei observables with $Z \geq 8$ and to obtain a description of nuclear matter that follows the DBHF tendencies better than the conventional non-linear $\sigma - \omega$ models. To do that we will investigate the effects of the new couplings from EFT keeping the equilibrium properties fixed to those of TM1. It should be pointed out that, actually, the equilibrium properties of TM1 lie in the range for which a reasonable description of finite nuclei properties can be achieved, provided that the EFT parameters of the model are natural [15]. Here one has to note that the specific values of TM1 vary from the DBHF result. However, the RMF sets with only scalar self-interactions which give good saturation properties deviate sharply from DBHF at high density. Thus, for our purposes, we believe that a good way to settle

the parametrization is to remain close to the empirical value near saturation and follow an equation of state similar to that of the DBHF theory. In the next section we shall detail our strategy.

We emphasize that our goal is not to produce a new optimal set of parameters intended to compete with well-established conventional sets like NL3 [28], which already are very successful for nuclei both at and away from the line of β -stability. Instead, we wish to learn the possibilities of the new EFT models for describing finite nuclei and for simultaneously tuning the behaviour with density of the scalar and vector self-energies. In doing this we want to ascertain whether the comparison with DBHF can provide useful constraints on the new couplings. For our study, the determination of the parameters of the model through a least-squares fitting procedure, by calculating nuclear properties repeatedly until obtaining a best fit, would make the connections between the resulting parameters and the considered nuclear observables more obscure.

The paper is organized as follows. Section 2 is devoted to a summary of the mean field equations and to fit part of the parameters of the effective Lagrangian to nuclear matter data. We compare our results with the predictions of other parametrizations available in the literature. In the third section the remaining parameters of the effective Lagrangian are obtained by imposing that our mean field approach reproduces the experimental data for some selected nuclei. A BCS-type pairing correlation is added in Section 4 to calculate non-magic even-even nuclei. The extended parameter set is tested in some applications to nuclear structure phenomena like isotopic/isotonic energy differences, the isotopic change in the charge radius and nuclei with large neutron/proton excess. Finally, the summary and concluding remarks are given in Section 5.

2 Nuclear matter

The RMF treatment of the QHD models automatically includes the spin-orbit force, the finite range and the density dependence of the nuclear interaction. The RMF model has the advantage that, with the proper relativistic kinematics and with the meson properties already known or fixed from the properties of a small number of finite nuclei, gives excellent results for binding energies, root-mean-square radii, quadrupole and hexadecapole deformations and other properties of spherical and deformed nuclei [26,28,29,30,31]. The quality of the results is comparable to that found in non-relativistic nuclear structure calculations with effective Skyrme [32] or Gogny [33] forces.

In recent years the effective field theory approach to QHD has been studied extensively. The theory and the equations for finite nuclei and nuclear matter can be found in the literature [7,10,11,12] and we shall only outline the formalism here. We start from Ref. [10] where the field equations were derived from an energy density functional containing Dirac baryons and classical scalar and vector mesons. Although this energy functional can be obtained from the effective Lagrangian in the Hartree approximation [7,11], it can also be considered as an expansion in terms of ratios of the meson fields and their gradients to the nucleon mass of a general energy density functional that contains the contributions of correlations within the spirit of density functional theory.

According to Refs. [7,11,12] this energy density functional for finite nuclei can be written as

$$\begin{aligned}
\mathcal{E}(r) = & \sum_{\alpha} \varphi_{\alpha}^{\dagger}(r) \left\{ -i\boldsymbol{\alpha} \cdot \boldsymbol{\nabla} + \beta[M - \Phi(r)] + W(r) + \frac{1}{2}\tau_3 R(r) + \frac{1 + \tau_3}{2}A(r) \right. \\
& \left. - \frac{i\beta\boldsymbol{\alpha}}{2M} \cdot \left(f_v \boldsymbol{\nabla} W(r) + \frac{1}{2} f_{\rho} \tau_3 \boldsymbol{\nabla} R(r) \right) \right\} \varphi_{\alpha}(r) \\
& + \left(\frac{1}{2} + \frac{\kappa_3}{3!} \frac{\Phi(r)}{M} + \frac{\kappa_4}{4!} \frac{\Phi^2(r)}{M^2} \right) \frac{m_s^2}{g_s^2} \Phi^2(r) - \frac{\zeta_0}{4!} \frac{1}{g_v^2} W^4(r) \\
& + \frac{1}{2g_s^2} \left(1 + \alpha_1 \frac{\Phi(r)}{M} \right) (\boldsymbol{\nabla} \Phi(r))^2 - \frac{1}{2g_v^2} \left(1 + \alpha_2 \frac{\Phi(r)}{M} \right) (\boldsymbol{\nabla} W(r))^2 \\
& - \frac{1}{2} \left(1 + \eta_1 \frac{\Phi(r)}{M} + \frac{\eta_2}{2} \frac{\Phi^2(r)}{M^2} \right) \frac{m_v^2}{g_v^2} W^2(r) - \frac{1}{2e^2} (\boldsymbol{\nabla} A(r))^2
\end{aligned}$$

$$-\frac{1}{2g_\rho^2}(\nabla R(r))^2 - \frac{1}{2}\left(1 + \eta_\rho \frac{\Phi(r)}{M}\right) \frac{m_\rho^2}{g_\rho^2} R^2(r), \quad (2.1)$$

where the index α runs over all occupied states of the positive energy spectrum, $\Phi \equiv g_s \phi_0$, $W \equiv g_v V_0$, $R \equiv g_\rho b_0$ and $A \equiv eA_0$. Except for the terms with α_1 and α_2 , the functional (2.1) is of fourth order in the expansion. Following Refs. [7,11,16], we retain the fifth-order terms α_1 and α_2 because their contribution to the nuclear surface energy is numerically of the same magnitude as the contribution from the quartic scalar term. One can see that the new terms concentrate on the isoscalar channel and that the expansion with respect to the isovector meson is shorter (the η_ρ coupling is of third order). Higher non-linear couplings of the ρ meson are not considered because the expectation value of the ρ field is typically an order of magnitude smaller than that of the ω field [7,11], and they only have a marginal impact on the usual properties studied for terrestrial nuclei. For example, in calculations of the high-density equation of state, Müller and Serot [12] found the effects of a quartic ρ meson coupling (R^4) to be appreciable only in stars made of pure neutron matter. A surface contribution $-\alpha_3 \Phi (\nabla R)^2 / (2g_\rho^2 M)$ was tested in Ref. [16] and it was found to have absolutely negligible effects. We should note, nevertheless, that very recently it has been shown that couplings of the type $\Phi^2 R^2$ and $W^2 R^2$ are useful to modify the neutron radius in heavy nuclei while making very small changes to the proton radius and the binding energy [34].

The Dirac equation corresponding to the energy density (2.1) becomes

$$\left\{ -i\boldsymbol{\alpha} \cdot \nabla + \beta[M - \Phi(r)] + W(r) + \frac{1}{2}\tau_3 R(r) + \frac{1 + \tau_3}{2} A(r) - \frac{i\beta\boldsymbol{\alpha}}{2M} \cdot \left[f_v \nabla W(r) + \frac{1}{2} f_\rho \tau_3 \nabla R(r) \right] \right\} \varphi_\alpha(r) = \varepsilon_\alpha \varphi_\alpha(r). \quad (2.2)$$

The mean field equations for Φ , W , R and A are given by

$$\begin{aligned} -\Delta\Phi(r) + m_s^2\Phi(r) &= g_s^2 \rho_s(r) - \frac{m_s^2}{M} \Phi^2(r) \left(\frac{\kappa_3}{2} + \frac{\kappa_4}{3!} \frac{\Phi(r)}{M} \right) \\ &+ \frac{g_s^2}{2M} \left(\eta_1 + \eta_2 \frac{\Phi(r)}{M} \right) \frac{m_v^2}{g_v^2} W^2(r) + \frac{\eta_\rho}{2M} \frac{g_s^2}{g_\rho^2} m_\rho^2 R^2(r) \\ &+ \frac{\alpha_1}{2M} [(\nabla\Phi(r))^2 + 2\Phi(r)\Delta\Phi(r)] + \frac{\alpha_2}{2M} \frac{g_s^2}{g_v^2} (\nabla W(r))^2, \quad (2.3) \end{aligned}$$

$$-\Delta W(r) + m_v^2 W(r) = g_v^2 \left(\rho(r) + \frac{f_v}{2} \rho_T(r) \right) - \left(\eta_1 + \frac{\eta_2}{2} \frac{\Phi(r)}{M} \right) \frac{\Phi(r)}{M} m_v^2 W(r)$$

$$-\frac{1}{3!}\zeta_0 W^3(r) + \frac{\alpha_2}{M}[\nabla\Phi(r) \cdot \nabla W(r) + \Phi(r)\Delta W(r)], \quad (2.4)$$

$$-\Delta R(r) + m_\rho^2 R(r) = \frac{1}{2}g_\rho^2 \left(\rho_3(r) + \frac{1}{2}f_\rho \rho_{T,3}(r) \right) - \eta_\rho \frac{\Phi(r)}{M} m_\rho^2 R(r), \quad (2.5)$$

$$-\Delta A(r) = e^2 \rho_p(r), \quad (2.6)$$

where the baryon, scalar, isovector, proton and tensor densities are

$$\rho(r) = \sum_\alpha \varphi_\alpha^\dagger(r) \varphi_\alpha(r), \quad (2.7)$$

$$\rho_s(r) = \sum_\alpha \varphi_\alpha^\dagger(r) \beta \varphi_\alpha(r), \quad (2.8)$$

$$\rho_3(r) = \sum_\alpha \varphi_\alpha^\dagger(r) \tau_3 \varphi_\alpha(r), \quad (2.9)$$

$$\rho_p(r) = \sum_\alpha \varphi_\alpha^\dagger(r) \left(\frac{1 + \tau_3}{2} \right) \varphi_\alpha(r), \quad (2.10)$$

$$\rho_T(r) = \sum_\alpha \frac{i}{M} \nabla \cdot [\varphi_\alpha^\dagger(r) \beta \boldsymbol{\alpha} \varphi_\alpha(r)], \quad (2.11)$$

$$\rho_{T,3}(r) = \sum_\alpha \frac{i}{M} \nabla \cdot [\varphi_\alpha^\dagger(r) \beta \boldsymbol{\alpha} \tau_3 \varphi_\alpha(r)]. \quad (2.12)$$

In the context of density functional theory it is possible to parametrize the exchange and correlation effects through local potentials (Kohn–Sham potentials), as long as those contributions be small enough that can be considered as minor perturbations to the potentials [35]. As it is known, this is the case with the local meson fields. The Hartree values are the ones that control the dynamics in the relativistic DBHF calculations. Therefore, the meson fields can also be interpreted as Kohn–Sham potentials. Equations (2.3)–(2.6) thus correspond to the Kohn–Sham equations in the relativistic case [36] and in this sense they include effects beyond the Hartree approach through the non-linear couplings [7,10,11].

For infinite nuclear matter all of the gradients of the fields in Eqs. (2.1)–(2.6) vanish and only the κ_3 , κ_4 , η_1 , η_2 and ζ_0 non-linear couplings remain. Due to the fact that the solution of symmetric nuclear matter in mean field depends on the ratios g_s^2/m_s^2 and g_v^2/m_v^2 [6], we have seven unknown parameters. By imposing the values of the saturation density, total energy, incompressibility modulus and effective mass, we still have three free parameters (the value of g_ρ^2/m_ρ^2 is fixed from the bulk symmetry energy coefficient J).

A possible starting point for our study of the effects of the new terms in the EFT energy

density, as mentioned in the Introduction, is the TM1 parametrization [25]. First, because it nicely agrees with the DBHF calculations with the Bonn-A potential [37] for a wide range of densities. And second, because it provides good results when applied to finite nuclei calculations, even far away from the β -stability line. Our aim is to study the effects of the new couplings in the description of nuclear matter and finite nuclei and, at the same time, to improve the TM1 parametrization. Then, instead of determining the whole set of parameters by a least-squares fit, we will follow a step-by-step strategy, similar to the one used to determine the parameter sets in Refs. [38,39] in the relativistic framework, or to determine the Skyrme SkM* parametrization [40] in the non-relativistic case.

According to this strategy we first fix the saturation properties to be those of TM1 and then introduce the coupling ζ_0 and the new scalar-vector non-linear couplings η_1 and η_2 . This way we can make sure, broadly speaking, that we have the same behaviour of the equation of state around the saturation point as with TM1. The addition of the couplings ζ_0 , η_1 and η_2 cannot be done with complete freedom once the saturation properties have been fixed. Including these extra couplings is translated into a modification of the other coefficients which, eventually, may be driven to non-natural values. An enlarged discussion of this effect can be found in Ref. [16]. To keep all the coefficients within natural values we find that $\zeta_0 = 3.6$, $\eta_1 = 1.1$ and $\eta_2 = 0.1$ is a good choice. It furthermore produces an equation of state and self-energies in better agreement with DBHF than TM1 (and also contributes to improve the results for ^{16}O that is one of the weak points of TM1, see Section 3). The values of the coupling constants along with the saturation properties are collected in Table 1. We have denoted this set of parameters as TM1*. We can see that κ_4 is positive and that all the coefficients are natural, i.e., $\mathcal{O}(1)$. The fact that κ_4 takes a positive value is very gratifying. Otherwise the energy spectrum has no lower bound and instabilities in calculations of the equation of state and of finite systems may occur [41].

Figure 1 displays the scalar U_s and vector U_v potentials as a function of the nuclear matter density calculated with TM1*, TM1 (that contains a quartic vector self-interaction but not the new couplings) and with the generalized sets G1 and G2 of Ref. [11] (effective field theory model), in comparison with the DBHF result. We also show the results obtained with the NL3 parameter set [28] that we have chosen as a representative of the usual non-linear $\sigma - \omega$ parametrizations with only scalar self-interactions. Note that the κ_4 term of NL3 bears a negative sign (Table 1). Figure 2 shows the equation of state for the different approaches. The DBHF predictions are believed to be realistic up to a density, typically, around twice

the saturation density [25].

From Figures 1 and 2 it is clear that the cubic and quartic self-interactions play a crucial role in following the DBHF results at high density. The standard non-linear $\sigma - \omega$ sets such as NL3 completely fail in doing so: the vector potential grows almost like a straight line and gives a much too stiff equation of state. The quartic vector self-interaction brings down the vector potential and makes the equation of state softer. This softening of the high-density equation of state is needed to be consistent with the observed neutron star masses [12]. By construction TM1* gives the same saturation properties as TM1. However, including the meson interactions η_1 and η_2 we have been able to reproduce the DBHF results with TM1* better than with TM1, for moderate and high densities. We have checked that if one tries to reproduce the DBHF results setting $\eta_1 = \eta_2 = 0$ this favours large non-natural values of ζ_0 . If we set $\eta_1 = \eta_2 = 0$ and ζ_0 is small (roughly < 2) then κ_4 remains negative. Only by introducing the extra constants η_1 and η_2 one can agree better with DBHF, have $\kappa_4 > 0$ and a not very large ζ_0 value. Nevertheless, we have found that the contributions of the third-order term $\eta_1 \Phi W^2$ and of the fourth-order term $\zeta_0 W^4$ in the energy density are far more important than the contribution of the quartic term $\eta_2 \Phi^2 W^2$. In fact, we underline that in our calculation η_2 is compatible with a vanishing value, indicating that the comparison with DBHF serves to fix only two couplings of the triad $(\zeta_0, \eta_1, \eta_2)$. On the other hand, the generalized G1 and G2 sets (that were obtained by fitting finite nuclei observables different from the ones used in TM1) also show a good agreement with the DBHF results. From Figures 1 and 2 one can see that the results obtained with G1 are similar to those of TM1, while the predictions of G2 are closer to DBHF.

3 Finite nuclei

In finite nuclei the contributions from the couplings α_1 and α_2 between the scalar field and the gradients of the vector and scalar fields, as well as the tensor couplings f_v and f_ρ of the ω and ρ mesons to the nucleon, do not vanish. Therefore, we have in principle four more parameters to adjust, plus the masses of the σ , ω and ρ mesons (or, equivalently, the coupling constants g_s , g_v and g_ρ). In accordance with our strategy, we will fix the meson masses of TM1* to the same values of TM1: $m_s = 511.198$ MeV, $m_\omega = 783$ MeV and $m_\rho = 770$ MeV (the nucleon mass is $M = 938$ MeV). In this way we do not mask the influence of the terms that we want to study.

In our numerical calculation of finite nuclei we have transformed the Dirac equation (2.2) into a Schrödinger-like equation by eliminating the small component of the wave function. This equation is solved by using a standard code for non-relativistic Skyrme–Hartree–Fock calculations [32]. In the calculations performed with the improved TM1 set (TM1*) we use the same center-of-mass correction for energies and charge radii as Sugahara and Toki [25] used for TM1:

$$E_{\text{CM}} = \frac{3}{4}\hbar\omega, \quad r_{\text{ch}}^2 = r_{\text{p}}^2 + 0.64 - \frac{3}{2} \left(\frac{b^2}{A} \right) \text{ fm}^2, \quad (3.1)$$

where $\hbar\omega = 41A^{-1/3}$ MeV, $b = \sqrt{\hbar/m\omega}$ is the harmonic oscillator parameter and 0.64 fm^2 takes into account the finite size correction of the proton [42].

We obtain the coupling constants α_1 , α_2 , f_v , ζ_0 , η_1 and η_2 (the last three combined with the nuclear matter calculation as explained in Section 2) by imposing that the total energy, the charge radius and the $1p$ splitting for neutrons and protons of the symmetric nucleus ^{16}O be as close as possible to the experimental values. To deal with asymmetric nuclei the g_ρ , η_ρ and f_ρ couplings are needed. Following Ref. [25] we fix the volume asymmetry coefficient

$$J = \frac{k_F^2}{6(k_F^2 + M_\infty^*)^{1/2}} + \frac{g_\rho^2 k_F^2}{12\pi^2 m_\rho^2} \frac{1}{1 + \eta_\rho(1 - M_\infty^*/M)} \quad (3.2)$$

to be 36.9 MeV. Actually this value corresponds to the difference between the neutron and nuclear matter DBHF energies per particle [43] calculated at the nuclear matter saturation density, which is known to be a good approach for estimating J [44]. Then we determine η_ρ and f_ρ so that the energy of ^{208}Pb be the experimental one. The tensor coupling f_ρ happens to be useless in our fitting: its contribution, as previously reported [16,30], is negligible and we have taken $f_\rho = 0$ for TM1*. This is not the case for the coupling η_ρ , whose influence is

noticeable [16]. As a final step in our fitting procedure we have to check that the values of all the parameters are natural. The whole set of parameters of TM1* is given in Table 1.

We should like to discuss the systematics of the finite nuclei properties with the new couplings in some more detail. The bulk parameters $(\zeta_0, \eta_1, \eta_2)$ only have a slight influence on the binding energies (B) and charge radii (r_{ch}), and practically no effect on the spin-orbit splittings (ΔE_{SO}). The incidence of η_2 is again negligible compared to ζ_0 and η_1 . However, if $(\zeta_0, \eta_1, \eta_2)$ are given the wrong values then it may be impossible to correct the results for B and r_{ch} with only the surface parameters $(f_v, \alpha_1, \alpha_2)$. Thus, one first needs a reasonable ansatz for $(\zeta_0, \eta_1, \eta_2)$ to be able to get acceptable values for B and r_{ch} . It was not obvious a priori that the $(\zeta_0, \eta_1, \eta_2)$ values favoured by the comparison with DBHF would fall into this category. If all other parameters are kept fixed, decreasing α_1 makes B and ΔE_{SO} larger and r_{ch} smaller (we define B to be positive). The coupling α_2 has just the opposite effect. For the same change in α_1 as in α_2 , the modifications on B , r_{ch} and ΔE_{SO} are roughly twice larger with α_1 than with α_2 . Once a set of $(\zeta_0, \eta_1, \eta_2)$ values is specified, f_v serves to bring the strength of ΔE_{SO} closer to the desired value. Then the couplings α_1 and α_2 are used for the fine tuning of the B , r_{ch} and ΔE_{SO} values. We point out that after specifying $(\zeta_0, \eta_1, \eta_2)$ almost the same B , r_{ch} and ΔE_{SO} are obtained with many distinct families of (α_1, α_2) values. In principle, we have realized that making α_1 small or negative and readjusting α_2 to recover the same binding energies and spin-orbit splittings, helps one to eventually get slightly larger radii. That is, from the interplay of α_1 and α_2 it is possible to achieve some change in the value of r_{ch} relative to the value of B , but the effect is not very significant. We are led to conclude that at least one of the three couplings $(f_v, \alpha_1, \alpha_2)$ is not singled out by the properties analyzed, and that a correlation exists between these surface parameters and the bulk parameters $(\zeta_0, \eta_1, \eta_2)$.

As a first test of the full TM1* parametrization we have calculated the surface energy coefficient E_s and the surface thickness t of the density profile (standard 90%-10% fall-off distance of the nuclear density) in semi-infinite nuclear matter. The results are shown in Table 2. The surface energy obtained with TM1* lies within the region of empirical values, whereas the surface thickness t is slightly small [16,45]. The energies, charge radii and spin-orbit splittings of the magic nuclei ^{16}O and ^{208}Pb used in our fit as well as the values for ^{40}Ca , ^{48}Ca and ^{90}Zr , which were included in the fit of TM1 [25], are also displayed in Table 2. We show the experimental values and the results obtained with the sets TM1*, TM1 and NL3 [28] (non-linear model with only scalar self-interactions), and with the generalized

parameter sets G1 and G2 of Ref. [11]. In addition to the couplings listed in Table 1 for G1 and G2, these sets have a few more parameters related with the electromagnetic structure of the pion and the nucleon (see Ref. [11]), which we have taken into account for Table 2. The TM1 results for ^{16}O are given here for completeness, as we recall that TM1 was devised for heavier nuclei [25]. Concerning the influence of the centre-of-mass motion on the energy and the charge radius, it should be noted that different parametrizations use, in general, different prescriptions. Due to the fact that the centre-of-mass corrections are included in the fit of the parameters, we report in Table 2 the values we have obtained with the same prescription as the authors used in their original works.

The TM1* calculations for magic nuclei displayed in Table 2 reproduce the experimental energies within $\sim 0.8\%$ and the charge radii and spin-orbit splittings with a similar quality to the successful NL3 [28], G1 or G2 [11] parametrizations. In order to check the ability of TM1* for describing nuclei far from the stability line, we have calculated the energy and charge radius of some drip-line (double-closed shell) nuclei, namely ^{56}Ni , ^{78}Ni , ^{100}Sn and ^{132}Sn . Table 2 shows that all the forces considered here produce similar results for the energy per particle and the charge radius of finite nuclei, which agree well with experiment. The single-particle energies of neutrons and protons are compared with the experimental data in Figures 3a and 3b for the ^{208}Pb nucleus with the TM1*, TM1 and NL3 sets. One can see that all these parametrizations qualitatively describe the experimental values. Although the nuclear matter properties are equal in TM1 and TM1*, the spectra are slightly different mainly due to the tensor coupling f_v present in TM1*, which has a noticeable influence in the spin-orbit potential [7,10,16,17].

4 Even-even nuclei

To describe even-even nuclei other than double magic nuclei we introduce the pairing correlation in the BCS approximation with a constant gap Δ , as in earlier calculations [25,26,29]. It is to be kept in mind that the seniority pairing recipe is not appropriate for exotic nuclei near the drip lines because the coupling to the continuum is not treated properly. The fact that continuum states become significantly populated as one approaches the drip lines can be taken into account in the relativistic Hartree-plus-Bogoliubov (RHB) method [46,47,48]. However, it has been pointed out in Ref. [49] that a qualitative estimation of the drip lines can be obtained within the BCS scheme by taking into account some quasi-bound states owing to their centrifugal barrier which mocks up the influence of the continuum.

In order to be as consistent as possible with TM1 here we take the gap energy $\Delta = 11.2/\sqrt{A}$ MeV, that corresponds to the widely used phenomenological formula of Bohr and Mottelson [50]. In practice we have found that the same gap energy is obtained by fitting the Sn isotopic energy difference [49]

$$\Delta E = [E - E(^{116}\text{Sn})]_{\text{BCS}} - [E - E(^{116}\text{Sn})]_{\text{Exp}}. \quad (4.1)$$

calculated with TM1*. We restrict the number of active shells to the occupied shells contained in a major harmonic oscillator shell above and below of the last closed shell. When the nuclei approach the drip lines there are not bound single-particle levels above the chemical potential. In this case we take the bound-state contributions as well as those coming from quasi-bound states at positive energies [49].

In Table 3 we report the energy and charge radii of ^{58}Ni , $^{116,124}\text{Sn}$ and $^{184,196,214}\text{Pb}$ that were used in the TM1 fit. TM1* shows an agreement with experiment similar to that found for TM1. Apart from the results presented in Tables 2 and 3, we have compared the energy given by TM1* for several light nuclei of $Z \leq 20$ with the results given by TM2 [25] (as TM2 was designed for $Z \leq 20$) and with the TM1 results. TM1* improves the TM1 results in this region and the quality of the energies is similar to that of TM2. In the following we will calculate isotopic and isotonic energy differences, isotopic shifts in charge radii and two-neutron and two-proton separation energies near and away from the β -stability line, to examine whether TM1* is also acceptable for these properties in comparison with experiment and with other relativistic sets.

4.1 Isotopic and isotonic energy differences

We have calculated the isotopic energy differences ΔE for several Sn and Pb isotopes (referred to ^{116}Sn and ^{208}Pb , respectively) with the TM1*, TM1 and NL3 parametrizations. The results are shown in Figures 4a and 4b. In the case of the Sn isotopes there are some differences between the NL3 results and those of TM1 or TM1*. The NL3 isotopic energy differences appreciably deviate from the experiment for Sn isotopes with a neutron number N larger than 66, while the TM1 or TM1* results remain close to the experimental values. If we compare with the non-relativistic calculations performed in Ref. [49] with the Skyrme forces SLy4 and SkM*, the NL3 results qualitatively behave as those of SkM*, whereas the TM1 and TM1* predictions are closer to those of SLy4. The results for the Pb isotopes are shown in Figure 4b, and for $N = 82$ isotones (referred to ^{132}Sn) in Figure 4c. The TM1*, TM1 and NL3 sets show different trends for the lead isotopes. TM1 predicts better ΔE values over the other parameter sets. For the $N < 126$ isotopes TM1 and TM1* predict an arch structure similar to the one found with the SLy4 interaction [49], while NL3 shows a structure more similar to the SkM* force [49]. For $N > 126$, ΔE increases as a function of N for the three relativistic sets, similarly to the SLy4 calculation [49].

The $N = 82$ isotone energy differences found with NL3, TM1 and TM1* show a completely different behaviour compared with SLy4 and SkM*. In the relativistic case ΔE decreases with increasing Z up to $Z = 56$ and increases afterwards. The largest separation with respect to the experimental value corresponds to $Z = 56$, although the difference is more pronounced for TM1 and TM1* than for NL3. In the non-relativistic calculations [49] one finds an arch structure with SLy4, with the largest difference with experiment corresponding to $Z = 56$ (although it is positive in this case), and a monotonous increasing of ΔE as a function of Z with SkM*. This qualitatively different behaviour in the $N = 82$ isotopic chain could be caused by the different pairing interaction used in the present calculation (constant gap) and in the non-relativistic calculations of Ref. [49] where a density-dependent zero-range pairing force (more similar to a constant strength) was considered.

4.2 Isotopic change in charge radius

In the past years the isotopic shifts in charge radii have been studied for the isotopic chain of Pb nuclei using various techniques [49,51,52]. Non-linear $\sigma - \omega$ calculations with a constant gap pairing interaction in general reproduce the experimentally observed kink in the isotopic

shifts about ^{208}Pb [28,52]. However, the standard non-relativistic (zero range or finite range) forces are not able to describe this kink. Only by improving the pairing interaction and by taking into account some terms usually not considered in the Skyrme functional and the two-body center-of-mass correction, the non-relativistic results agree with the experimental observation [49,51]. Here we have calculated the Pb isotopic shifts with the TM1* parameter set. In Figure 5 the result is compared with the prediction of the TM1 and NL3 sets, and also with the experimental data. All these parameter sets yield qualitatively similar results and reproduce the experimental kink reasonably well. Notice that these Pb isotopic shifts are not included in the TM1 and TM1* fits.

4.3 Two-neutron and two-proton separation energies

We have evaluated the two-neutron S_{2n} and two-proton S_{2p} separation energies from the calculated energies using [50]

$$S_{2n}(N, Z) = E(N - 2, Z) - E(N, Z), \quad (4.2)$$

$$S_{2p}(N, Z) = E(N, Z - 2) - E(N, Z). \quad (4.3)$$

The S_{2n} values for the illustrative cases of $Z = 20$ and 50 as well as the S_{2p} value for $N = 82$ with the TM1*, NL3 and TM1 sets are presented in Figures 6a, 6b and 6c, respectively. The experimental data are also given for comparison.

On the whole, the S_{2n} and S_{2p} values obtained from TM1* agree well with the experimental observation and also with the predictions of TM1 and NL3 (except for a slight discrepancy for some specific cases). In concrete, for Ca isotopes the shell effects at $N = 20$ and 28 are well reproduced by the three relativistic sets. Another shell effect is predicted at $N = 38$ although no experimental information is available to confirm it. Something similar happens for Sn isotopes at $N = 50$ and at $N = 82$ where the calculated results qualitatively agree with the experimental value. With respect to the isotone chain of $N = 82$ no experimental information exists to confirm the shell effect at $Z = 50$. In this case the relativistic sets are not able to quantitatively reproduce the experimental S_{2p} energies in the $Z = 54$ – 58 region, due maybe to the adopted pairing scheme. The S_{2n} value decreases with increasing the neutron number and vanishes at the neutron-drip line. Similarly, the S_{2p} value decreases with increasing proton number as the proton-drip line is reached.

As we have mentioned, although the BCS approach to pairing correlations is not well

suited for dealing with the drip lines [46,47,48], an estimate can be given with the present BCS calculation that takes into account some continuum effects through the quasi-bound levels [49]. The authors of Ref. [25] discussed the inability of TM1 for describing Zr isotopes with N larger than 82, while they could be described with the NL1 parametrization. We have found that to be able to describe these nuclei, which have a chemical potential close to zero, it is crucial for the BCS calculation to take into account the quasi-bound levels $2f_{5/2}$, $1h_{9/2}$ and $1i_{13/2}$ that lie a few MeV above the Fermi level. In this way we have estimated the neutron-drip line for Zr at $N \sim 98$. Similarly, we have estimated the neutron-drip line for Ca, Sn and Pb isotopes at $A \sim 62$, 164 and 264, respectively, for all the analysed parameter sets. These BCS estimates are in good agreement with the results of the non-relativistic interactions SLy4 and SkM* reported in Ref. [49], where almost the same technique was used for dealing with the pairing correlations. For $N = 82$ isotones we find the proton-drip line at $A \sim 156$, which corresponds to ^{156}W in agreement with experimental information [54].

5 Summary and conclusions

We have explored whether the parameter set TM1 [25] can be improved by adding new couplings that stem from the modern effective field theory approach to relativistic nuclear phenomenology. We have been concerned with analyzing the possibilities of the new couplings to ensure a reasonable agreement with the density dependence of the scalar and vector components of the DBHF self-energies, while performing well for finite nuclei. The extended parameter set has been called TM1*. It is able to reproduce ground-state properties of spherical nuclei for $Z \geq 8$ with a quality similar to conventional sets like NL1 or NL3, and with the appealing feature of having a positive quartic scalar self-coupling. This could not be achieved with the set TM1 which had to be restricted to Z larger than 20 in order to keep κ_4 positive [25]. It is important to note that this limitation seems to be common to any set of parameters containing only a quartic vector self-interaction on top of the standard non-linear $\sigma - \omega$ model. To check this point we have performed calculations with the recently proposed NL-SV1 and NL-SV2 parameter sets [48] that include a quartic vector self-coupling (like TM1). For light nuclei we find a good agreement with experiment when we use the NL-SV1 set which has a negative κ_4 coupling, whereas this is not the case with the NL-SV2 set where κ_4 is positive.

In comparison with the DBHF results in nuclear matter the extended set TM1* shows a significant improvement over TM1 due to the addition of the η_1 and η_2 couplings. The latter couplings (at least η_1) are very helpful to bring the vector and scalar potentials closer towards the DBHF calculations as the density grows. To the end of computing finite nuclei we have introduced the f_v , α_1 , α_2 , η_ρ and f_ρ parameters on top of the set that describes nuclear matter. We remark that the new parameters have a minor influence on the investigated properties of finite nuclei. However, they allow the full TM1* force to improve the agreement with experiment for double-closed shell nuclei compared with the starting TM1 parameters and to obtain better results for light-mass nuclei, which was a shortcoming of the TM1 set. We also have tested the TM1* force for isotopic energy differences, isotopic changes in charge radii and two-neutron and two-proton separation energies. Nuclei near the drip lines have been explored for some particular cases by taking into account quasi-bound states in the BCS calculation following the method of Ref. [49]. It should be mentioned that by including all of the relevant couplings in the energy density expansion compatible with the EFT approach to QHD, as developed in Refs. [7,11], the TM1* model is more consistent with our current

understanding of effective field theories. Nevertheless, we have seen that some of the new couplings of the EFT model remain underdetermined in spite of the information taken into account about the equation of state and the self-energies at higher densities.

In conclusion, the relativistic mean field approach extended by the new non-linear meson self-interactions and tensor couplings based upon effective field theory, allows one to reproduce at the same time the trends of microscopic DBHF calculations up to relatively high densities and various finite nuclei properties. In the low-density domain (that corresponds to the finite nuclei region) the main properties are almost fixed by the nuclear matter properties around saturation, and then the new parameters have only a small contribution. However, as the density increases the vector-vector and scalar-vector meson interactions play an important role in providing enough flexibility to the model to be able to follow the tendency of the DBHF calculations. Extended sets like TM1* may be more useful for systems having relatively higher density and temperature, whereas they will serve the same purpose for normal systems as the conventional parameter sets. To further constrain the new EFT parameters additional observables will be required. Nuclear phenomena involving currents could prove helpful for couplings such as α_1 and α_2 that imply the derivatives of the fields. On the side of the isovector channel, information from many-body DBHF calculations of asymmetric and neutron matter as well as data on neutron radii and the neutron skin thickness should be relevant.

6 Acknowledgements

The authors would like to acknowledge support from the DGICYT (Spain) under grant PB98-1247 and from DGR (Catalonia) under grant 1998SGR-00011. M.D.E. acknowledges financial support from the CIRIT (Catalonia). S.K.P. thanks the Spanish Education Ministry grant SB97-OL174874 for financial support and the Departament d'Estructura i Constituents de la Matèria of the University of Barcelona for kind hospitality.

References

- [1] R. Machleidt, *Adv. Nucl. Phys.* **19**, 189 (1989).
- [2] C. J. Horowitz and B. D. Serot, *Phys. Lett. B* **137**, 283 (1984).
- [3] M. R. Anastasio, L. S. Celenza, W. S. Pong, and C. M. Shakin, *Phys. Rep.* **100**, 327 (1983).
- [4] R. Brockmann and R. Machleidt, *Phys. Lett. B* **149**, 283 (1984).
- [5] B. ter Haar and R. Malfliet, *Phys. Rep.* **149**, 207 (1987).
- [6] B. D. Serot and J. D. Walecka, *Adv. Nucl. Phys.* **16**, 1 (1986).
- [7] B. D. Serot and J. D. Walecka, *Int. J. of Mod. Phys. E* **6**, 515 (1997).
- [8] J. D. Walecka, *Ann. Phys. (N.Y.)* **83**, 491 (1974).
- [9] J. Boguta and A. R. Bodmer, *Nucl. Phys.* **A292**, 413 (1977).
- [10] R. J. Furnstahl, B. D. Serot, and H. B. Tang, *Nucl. Phys.* **A598**, 539 (1996).
- [11] R. J. Furnstahl, B. D. Serot, and H. B. Tang, *Nucl. Phys.* **A615**, 441 (1997).
- [12] H. Müller and B. D. Serot, *Nucl. Phys.* **A606**, 508 (1996).
- [13] J. J. Rusnak and R. J. Furnstahl, *Nucl. Phys.* **A627**, 495 (1997).
- [14] B. C. Clark, R. J. Furnstahl, L. K. Kerr, J. Rusnak, and S. Hama, *Phys. Lett. B* **427**, 231 (1998).
- [15] R. J. Furnstahl and B. D. Serot, *Nucl. Phys.* **A671**, 447 (2000).
- [16] M. Del Estal, M. Centelles, and X. Viñas, *Nucl. Phys.* **A650**, 443 (1999).
- [17] R. J. Furnstahl, J. J. Rusnak, and B. D. Serot, *Nucl. Phys.* **A632**, 607 (1998).
- [18] P. Wang, *Phys. Rev. C* **61**, 054904 (2000).
- [19] F. Coester, S. Cohen, B. D. Day, and C. M. Vincent, *Phys. Rev. C* **1** 769 (1970).
- [20] A. Amorim and J. A. Tjon, *Phys. Rev. Lett.* **68**, 772 (1992).
- [21] S. Gmuca, *J. Phys. G* **17**, 1115 (1991).
- [22] M. Rashdan, *Phys. Lett. B* **395**, 141 (1997).
- [23] S. Gmuca, *Z. Phys. A* **342**, 387 (1992); *Nucl. Phys.* **A547**, 447 (1992).
- [24] A. R. Bodmer, *Nucl. Phys.* **A526**, 703 (1991); A. R. Bodmer and C. E. Price, *Nucl. Phys.* **A505**, 123 (1989).
- [25] Y. Sugahara and H. Toki, *Nucl. Phys.* **A579**, 557 (1994).
- [26] P. -G. Reinhard, M. Rufa, J. Maruhn, W. Greiner, and J. Friedrich, *Z. Phys. A* **323**, 13 (1986).
- [27] K. Sumiyoshi, H. Kuwabara, and H. Toki, *Nucl. Phys.* **A581**, 725 (1995).

- [28] G. A. Lalazissis, J. König, and P. Ring, *Phys. Rev. C* **55**, 540 (1997).
- [29] Y. K. Gambhir, P. Ring, and A. Thimet, *Ann. Phys. (N.Y.)* **198**, 132 (1990).
- [30] M. Rufa, P. -G. Reinhard, J. A. Maruhn, W. Greiner, and M. R. Strayer, *Phys. Rev. C* **38**, 390 (1988).
- [31] S. K. Patra and C. R. Praharaaj, *Phys. Rev. C* **44**, 2552 (1991).
- [32] D. Vautherin and D. M. Brink, *Phys. Rev. C* **5**, 626 (1972).
- [33] J. Dechargé and D. Gogny, *Phys. Rev. C* **21**, 1568 (1980).
- [34] C. J. Horowitz and J. Piekarewicz, *astro-ph/0010227* (2000).
- [35] W. Kohn and L. J. Sham, *Phys. Rev. A* **140**, 1133 (1965).
- [36] C. Speicher, R. M. Dreizler, and E. Engel, *Ann. Phys. (N.Y.)* **213**, 413 (1992).
- [37] R. Brockmann and R. Machleidt, *Phys. Rev. C* **42**, 1965 (1990).
- [38] C. J. Horowitz and B. D. Serot, *Nucl. Phys.* **A368**, 503 (1981).
- [39] A. Bouyssy, S. Marcos, and Pham Van Thieu, *Nucl. Phys.* **A422**, 541 (1984).
- [40] J. Bartel, P. Quentin, M. Brack, C. Guet, and H. -B. Håkansson, *Nucl. Phys.* **A386**, 79 (1982).
- [41] G. Baym, *Phys. Rev.* **117**, 886 (1960); B. M. Waldhauser, J. A. Maruhn, H. Stöcker, and W. Greiner, *Phys. Rev. C* **38**, 1003 (1988); P. -G. Reinhard, *Z. Phys. A* **329**, 257 (1988).
- [42] J. W. Negele, *Phys. Rev. C* **1**, 1260 (1970).
- [43] G. Q. Li, R. Machleidt, and R. Brockmann, *Phys. Rev. C* **45**, 2782 (1992).
- [44] L. Engvik, M. Hjorth-Jensen, R. Machleidt, H. Müther, and A. Polls, *Nucl. Phys.* **A627**, 85 (1997).
- [45] M. Centelles and X. Viñas, *Nucl. Phys.* **A563**, 173 (1993); M. Centelles, M. Del Estal, and X. Viñas, *Nucl. Phys.* **A635**, 193 (1998).
- [46] T. Gonzalez-Llarena, J. L. Egido, G. A. Lalazissis, and P. Ring, *Phys. Lett. B* **379**, 13 (1996).
- [47] G. A. Lalazissis, D. Vretenar, and P. Ring, *Phys. Rev. C* **57**, 2294 (1998).
- [48] M. M. Sharma, A. R. Farhan, and S. Mythili, *Phys. Rev. C* **61**, 054306 (2000).
- [49] E. Chabanat, P. Bonche, P. Haensel, J. Meyer, and R. Schaeffer, *Nucl. Phys.* **A635**, 231 (1998).
- [50] A. Bohr and B. R. Mottelson, “Nuclear Structure”, Vol. I (W.A. Benjamin, New York, 1969), Ch. 2.

- [51] N. Tajima, P. Bonche, H. Flocard, P. -H. Heenen, and M. S. Weiss, Nucl. Phys. **A551**, 434 (1993).
- [52] M. Sharma, G. A. Lalazissis, and P. Ring, Phys. Lett. B **317**, 9 (1993).
- [53] J. Dobaczewski, T. R. Werner, J. F. Berger, C. R. Chenn, and J. Decharge, Phys. Rev. C **53**, 2809 (1996); J. Terasaki, P. -H. Heenen, H. Flocard, and P. Bonche, Nucl. Phys. **A600**, 371 (1996).
- [54] R. D. Page, P. J. Woods, R. A. Cunningham, T. Davidson, N. J. Davis, S. Hofmann, A. N. James, K. Livingston, P. J. Sellin, and A. C. Shotter, Phys. Rev. Lett. **68**, 1287 (1992).

Figure captions

Figure 1. Scalar U_s and vector U_v potentials against the nuclear matter density as obtained in a DBHF calculation with the Bonn-A potential [37] and with the relativistic mean field parametrizations TM1*, TM1 [25], G1 and G2 [11].

Figure 2. Equation of state for the same cases as in Figure 1.

Figure 3. The single-particle energies for ^{208}Pb obtained by various relativistic mean-field parametrizations are compared with the experimental data for neutrons (a) and protons (b).

Figure 4. The isotopic energy difference obtained with the TM1* parameter set is compared with the TM1 and NL3 calculations for Sn isotopes (a) and Pb isotopes (b). Plot (c) shows the isotonic energy difference for $N = 82$.

Figure 5. The isotopic shifts in charge radii for the $Z = 82$ chain.

Figure 6. The calculated separation energies are compared with the experimental data: (a) two-neutron separation energy S_{2n} for $Z = 20$, (b) two-neutron separation energy for $Z = 50$, and (c) two-proton separation energy S_{2p} for $N = 82$.

Tables

Table 1: Various parameter sets for the relativistic energy density functional and the corresponding saturation properties. The coupling constants are dimensionless.

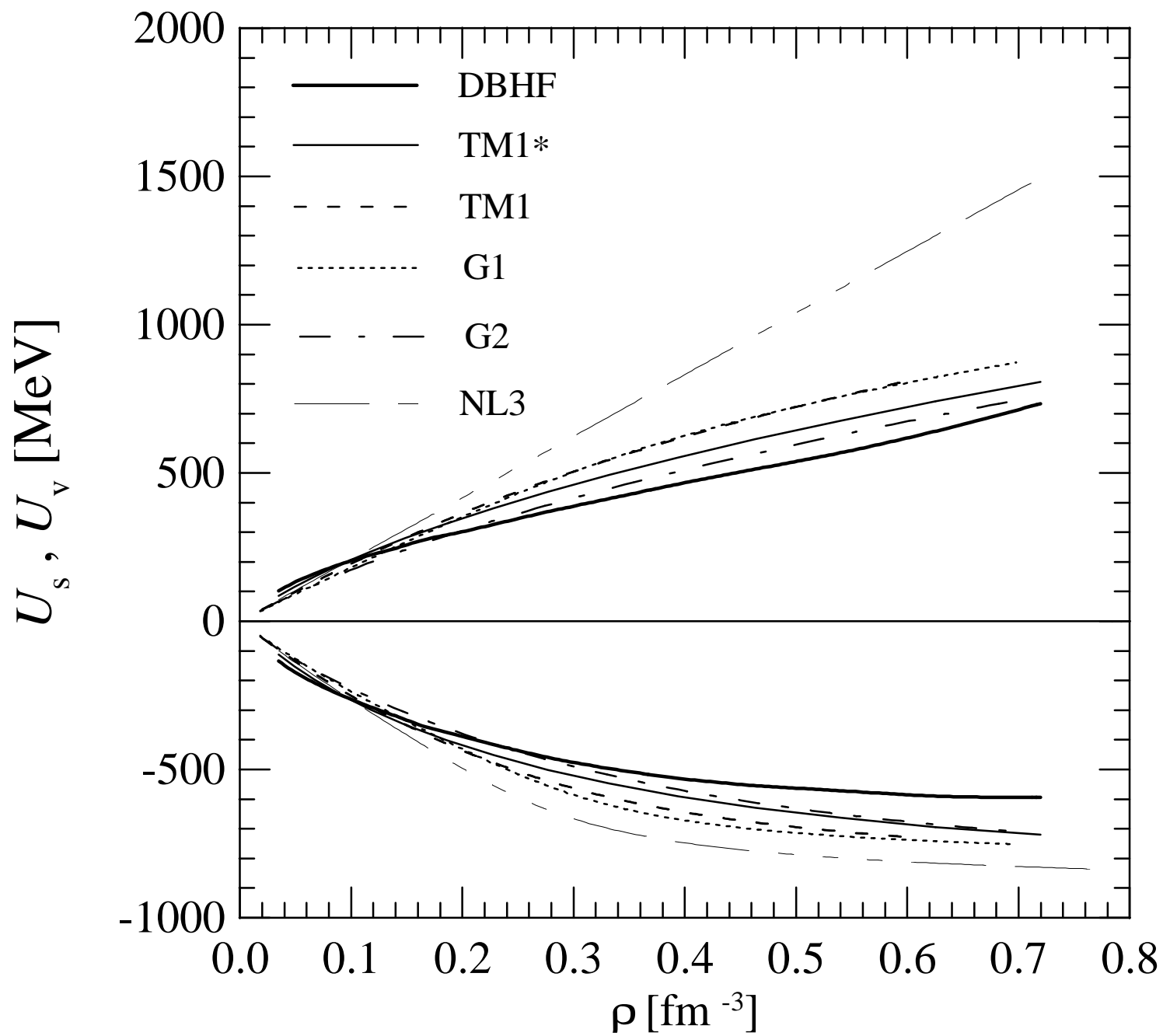
| | TM1* | TM1 | NL3 | G1 | G2 |
|-----------------------------------|--------|--------|--------|---------|--------|
| m_s/M | 0.545 | 0.545 | 0.541 | 0.540 | 0.554 |
| $g_s/4\pi$ | 0.893 | 0.798 | 0.813 | 0.785 | 0.835 |
| $g_v/4\pi$ | 1.192 | 1.003 | 1.024 | 0.9650 | 1.016 |
| $g_\rho/4\pi$ | 0.796 | 0.737 | 0.712 | 0.698 | 0.755 |
| κ_3 | 2.513 | 1.021 | 1.465 | 2.207 | 3.247 |
| κ_4 | 8.970 | 0.124 | -5.668 | -10.090 | 0.632 |
| ζ_0 | 3.600 | 2.689 | 0.0 | 3.525 | 2.642 |
| η_1 | 1.1 | 0.0 | 0.0 | 0.071 | 0.650 |
| η_2 | 0.1 | 0.0 | 0.0 | -0.962 | 0.110 |
| α_1 | -0.15 | 0.0 | 0.0 | 1.855 | 1.723 |
| α_2 | -2.20 | 0.0 | 0.0 | 1.788 | -1.580 |
| $f_v/4$ | 0.06 | 0.0 | 0.0 | 0.108 | 0.173 |
| η_ρ | 0.45 | 0.0 | 0.0 | -0.272 | 0.390 |
| a_v (MeV) | -16.30 | -16.30 | -16.24 | -16.14 | -16.07 |
| ρ_∞ (fm ⁻³) | 0.145 | 0.145 | 0.148 | 0.153 | 0.153 |
| K (MeV) | 281.1 | 281.1 | 271.5 | 215.0 | 215.0 |
| M_∞^*/M | 0.634 | 0.634 | 0.595 | 0.634 | 0.664 |
| J (MeV) | 36.90 | 36.90 | 37.40 | 38.5 | 36.4 |

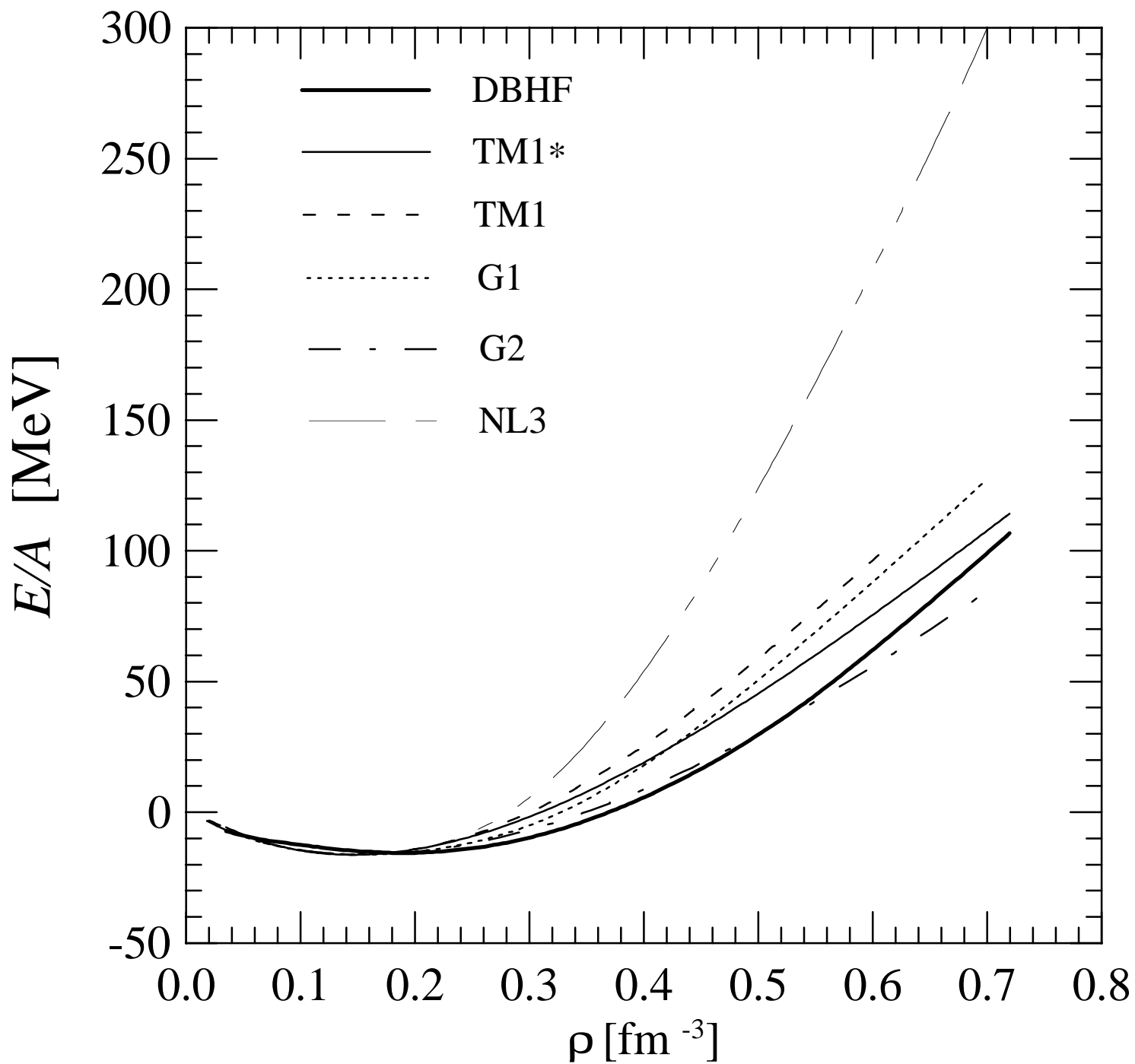
Table 2: The surface energy coefficient E_s , surface thickness t , energy per nucleon E/A , charge radius r_{ch} and spin-orbit splittings ΔE_{SO} of the least-bound nucleons using the TM1*, TM1, NL3, G1 and G2 parameter sets are compared with the experimental data. The energies are given in MeV, while t and r_{ch} are given in fm. The experimental values of E/A for ^{78}Ni and ^{100}Sn are, in fact, extrapolated data [49].

| | | TM1* | TM1 | NL3 | G1 | G2 | Exp. |
|-------------------|-------------------------------|-------|-------|-------|-------|-------|-----------|
| | E_s | 18.57 | 18.51 | 18.36 | 18.06 | 17.80 | 16.5–21.0 |
| | t | 1.90 | 1.91 | 1.99 | 1.98 | 2.08 | 2.2–2.5 |
| ^{16}O | E/A | -8.02 | -8.15 | -8.08 | -7.97 | -7.97 | -7.98 |
| | r_{ch} | 2.67 | 2.66 | 2.73 | 2.72 | 2.72 | 2.73 |
| | ΔE_{SO} (n,1p) | 6.3 | 5.6 | 6.4 | 6.0 | 5.9 | 6.2 |
| | (p,1p) | 6.2 | 5.6 | 6.3 | 5.9 | 5.9 | 6.3 |
| ^{40}Ca | E/A | -8.55 | -8.62 | -8.54 | -8.55 | -8.55 | -8.55 |
| | r_{ch} | 3.44 | 3.44 | 3.48 | 3.46 | 3.45 | 3.48 |
| | ΔE_{SO} (n,1d) | 6.3 | 5.7 | 6.7 | 6.6 | 6.5 | 6.3 |
| | (p,1d) | 6.3 | 5.7 | 6.6 | 6.5 | 6.4 | 7.2 |
| ^{48}Ca | E/A | -8.64 | -8.65 | -8.64 | -8.67 | -8.68 | -8.67 |
| | r_{ch} | 3.46 | 3.46 | 3.48 | 3.44 | 3.44 | 3.47 |
| | ΔE_{SO} (n,1d) | 5.4 | 5.0 | 6.1 | 5.8 | 5.6 | 3.6 |
| | (p,1d) | 5.6 | 5.2 | 6.3 | 6.2 | 6.0 | 4.3 |
| ^{90}Zr | E/A | -8.72 | -8.71 | -8.69 | -8.71 | -8.68 | -8.71 |
| | r_{ch} | 4.26 | 4.27 | 4.28 | 4.28 | 4.28 | 4.26 |
| | ΔE_{SO} (n,2p) | 1.6 | 1.4 | 1.6 | 1.8 | 1.8 | 0.5 |
| ^{208}Pb | E/A | -7.87 | -7.87 | -7.87 | -7.87 | -7.86 | -7.87 |
| | r_{ch} | 5.53 | 5.54 | 5.52 | 5.50 | 5.50 | 5.50 |
| | ΔE_{SO} (n,3p) | 0.8 | 0.7 | 0.8 | 0.9 | 0.9 | 0.9 |
| | (p,2d) | 1.7 | 1.4 | 1.6 | 1.8 | 1.8 | 1.3 |
| ^{56}Ni | E/A | -8.60 | -8.56 | -8.60 | -8.61 | -8.60 | -8.64 |
| | r_{ch} | 3.74 | 3.74 | 3.72 | 3.72 | 3.73 | 3.76 |
| ^{78}Ni | E/A | -8.18 | -8.19 | -8.23 | -8.28 | -8.28 | -8.23 |
| | r_{ch} | 3.95 | 3.95 | 3.95 | 3.92 | 3.92 | – |
| ^{100}Sn | E/A | -8.30 | -8.27 | -8.28 | -8.28 | -8.27 | -8.26 |
| | r_{ch} | 4.49 | 4.49 | 4.48 | 4.47 | 4.47 | – |
| ^{132}Sn | E/A | -8.33 | -8.34 | -8.36 | -8.38 | -8.37 | -8.35 |
| | r_{ch} | 4.72 | 4.73 | 4.72 | 4.69 | 4.69 | – |

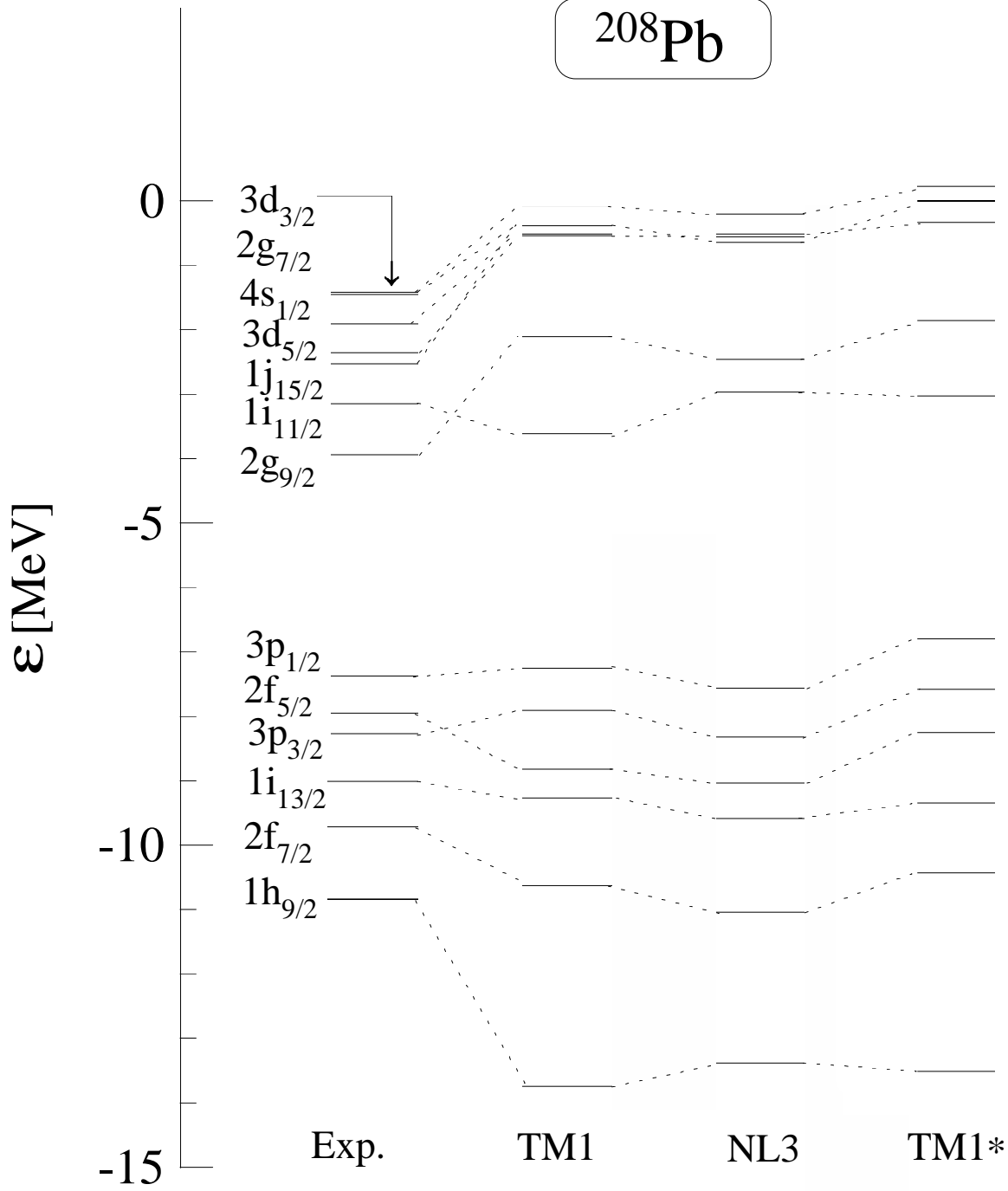
Table 3: Same as Table 2 for some open shell nuclei.

| | | TM1* | TM1 | NL3 | G1 | G2 | Exp. |
|-------------------|-----------------|-------|-------|-------|-------|-------|-------|
| ^{58}Ni | E/A | -8.64 | -8.61 | -8.63 | -8.62 | -8.62 | -8.73 |
| | r_{ch} | 3.76 | 3.76 | 3.75 | 3.74 | 3.75 | 3.77 |
| ^{116}Sn | E/A | -8.52 | -8.52 | -8.49 | -8.48 | -8.48 | -8.52 |
| | r_{ch} | 4.62 | 4.62 | 4.62 | 4.60 | 4.60 | 4.63 |
| ^{124}Sn | E/A | -8.45 | -8.46 | -8.45 | -8.46 | -8.45 | -8.47 |
| | r_{ch} | 4.67 | 4.67 | 4.67 | 4.65 | 4.64 | 4.67 |
| ^{184}Pb | E/A | -7.81 | -7.80 | -7.77 | -7.75 | -7.74 | -7.78 |
| | r_{ch} | 5.41 | 5.41 | 5.40 | 5.39 | 5.38 | - |
| ^{196}Pb | E/A | -7.89 | -7.87 | -7.86 | -7.85 | -7.84 | -7.87 |
| | r_{ch} | 5.47 | 5.48 | 5.46 | 5.45 | 5.44 | - |
| ^{214}Pb | E/A | -7.75 | -7.76 | -7.75 | -7.74 | -7.73 | -7.77 |
| | r_{ch} | 5.59 | 5.59 | 5.58 | 5.55 | 5.54 | - |





^{208}Pb



(a)

Neutrons

^{208}Pb

